ISSN 0016-7029, Geochemistry International, 2006, Vol. 44, No. 3, pp. 249–257. © Pleiades Publishing, Inc., 2006.
Original Russian Text © A.V. Ivanov, M.E. Zolensky, N.N. Kononkova, S.V. Yang, I.A. Stroganov, 2006, published in Geokhimiya, 2006, No. 3, pp. 284–292.

Kaidun Meteorite: Crystals of Oxides in Cavities

A. V. Ivanov*, M. E. Zolensky, N. N. Kononkova*, S. V. Yang***, and I. A. Stroganov***

** Vernadsky Institute of Geochemistry and Analytical Chemistry, Russian Academy of Sciences, ul. Kosygina 19, Moscow, 119991 Russia*
e-mail: andrei_ivanov@geokhi.ru
*** NASA Johnson Space Center, Houston, Texas 77058, United States*
**** Lockheed Engineering and Science Co., Houston, Texas 77058, United States*

Received March 9, 2004

Abstract—Cavities in two texturally and genetically distinct clasts of the Kaidun meteorite were found out to contain crystals of distinct morphology, but of a similar composition. Cavities in chondrite breccia #d3A contain thin (<4 μm) elongated (up to 25 μm long) crystals that grew perpendicular to the walls of the cavity. The walls of the cavities in partly fused clast #d(3-5)D are covered with clusters of acicular crystals. In both clasts, the crystals are covered by films of phyllosilicates and always have a composition approximated by the formula $(Mg,Fe,Mn)_5Al_2O_8 \cdot nH_2O$. No mineral phase of this composition has ever been found in nature. The genesis of the mineral phases in the cavities is thought to be related to the crystallization from a fluid of similar composition. The fluid was produced during the cooling of the melt that produced clast #d(3-5)D. The unusual composition of the crystals testifies that this fluid had an unusual composition. This can be explained by the unique nature of clast #d(3-5)D, for which there are good reasons to propose a Martian origin.

DOI: 10.1134/S0016702906030037

INTRODUCTION

Aqueous alterations of material at the parent body, a process associated with the transport of components and their deposition, was widespread at the parent bodies of carbonaceous chondrites, particularly those of low petrological types. The material of the Kaidun meteorite also shows numerous and diverse traces of this process. One of the most vivid (but not the only one) manifestations of this process is the aqueous alteration of metal and schreibersite in fragments of enstatite chondrites [1, 2]. The deposition of material during aqueous alterations at the parent bodies of carbonaceous chondrites is a fairly common process that was reportedly responsible for the development of phyllosilicate and carbonatite veinlets, which were also found in the Kaidun meteorite [3, 4].

This paper presents a description of crystals found in the cavities in two texturally and genetically distinct clasts of the Kaidun meteorite. The crystals notably differ in morphology but have similar compositions and, perhaps, geneses. No crystals of this composition have ever been found in nature.

CLAST #d3A

The clast has an equant shape, is about 2 mm across, and has a breccaited chondrule texture (Fig. 1). The boundaries between this clast and surrounding carbonaceous matrix are sharp. The texture of the chondrules is granular or, more rarely, barred. The porosity of the clast notably varies in its different parts.

The clast is composed essentially of olivine and pyroxene, whose grains broadly vary in size, from <10 μm to approximately 50 μm. The shape of the grains is usually irregular. Some of the olivine grains are included in the pyroxene grains. The clast contains aggregates of opaque minerals, which commonly have equant shapes and are as large as 250 μm. They consist of nickel-iron cores that are surrounded by outer sulfide

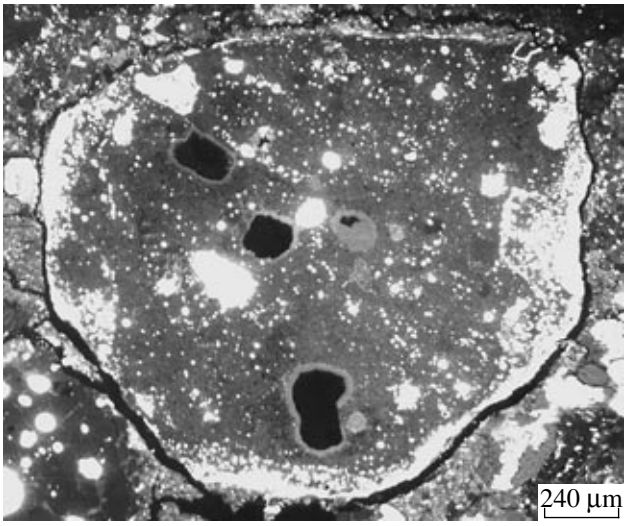

Fig. 1. Clast #d3A. BSE image. The clast contains visible cavities and aggregates of opaque minerals and is enriched in sulfides in the margins.

Table 1. Chemical composition (wt %, averages and ranges) of silicates in clast #3dA

Component	SiO_2	TiO_2	Al_2O_3	Cr_2O_3	FeO	MnO	MgO
Olivine	41.6	0.03	0.17	0.33	4.98	0.41	52.9
(*n* = 57)	39.1–42.9	<0.03–0.14	<0.03–0.69	0.12–0.82	0.41–7.49	<0.03–0.83	49.7–57.2
Low-Ca pyroxene	58.0	0.06	0.45	0.75	3.78	0.41	36.3
(*n* = 37)	55.4–59.8	0.03–0.13	0.17–1.25	0.27–0.94	0.45–5.74	0.05–0.53	33.4–38.9
Ca pyroxene	56.7	0.17	1.23	0.87	4.15	0.43	33.9
(*n* = 12)	54.0–59.0	0.09–0.35	0.47–2.59	0.44–1.18	1.04–7.52	0.18–0.55	31.7–36.1
High-Ca pyroxene	54.6	0.30	1.97	1.26	4.10	0.52	26.5
(*n* = 3)	54.2–55.0	0.27–0.33	1.52–2.77	1.20–1.35	3.43–5.31	0.48–0.56	25.0–28.0
Component	CaO	Na_2O	Total	Fo or En	Fa or Fs	Wo	FeO/MnO
Olivine	0.32	<0.03	100.74	94.5	5.5	–	14.3
(*n* = 57)	0.15–0.62	–		90.8–99.6	0.4–9.2		8.8–49.2
Low-Ca pyroxene	0.77	0.04	100.56	92.6	6.0	1.4	9.9
(*n* = 37)	0.15–1.62	<0.03–0.12		90.0–97.5	0.7–8.7	0.3–2.9	6.6–25.0
Ca pyroxene	2.63	0.09	100.17	88.4	6.7	4.9	10.0
(*n* = 12)	2.00–4.19	0.03–0.16		84.8–93.3	2.0–11.4	3.8–7.7	3.5–27.6
High-Ca pyroxene	10.6	0.24	100.09	72.2	7.1	20.7	7.8
(*n* = 3)	8.26–13.2	0.21–0.27		68.2–75.2	6.6–8.9	16.0–25.8	6.5–9.6

Note: *n* is the number of analyses; all Fe is recalculated to FeO.

rims. The peripheral parts of the clast are notably enriched in sulfide grains.

The olivine in this clast is magnesian (*Fa* 0.4–9.2, averaging 5.5). The composition of the pyroxene varies from enstatite to low-Ca augite (*Fs* 0.7–11.4). The compositions of the silicate phases of this clast are reported in Table 1. The nickel-iron commonly contains 7–9 wt % nickel. The clast also contains single grains of taenite (15 wt % Ni) and tetrataenite (49.4 wt % Ni). The sulfide rims around the nickel-iron contain troilite (0.3–0.9 wt % Ni) and pentlandite. Along the boundaries with sulfides, the nickel-iron commonly shows traces of aqueous alterations. The sulfides in the peripheral parts of the clast are troilite and pentlandite.

The brecciated texture of the clast testifies that this clast as a whole was not melted. This also follows from the compositions of the olivine and pyroxenes, which display significant variations in the concentrations of most components (Table 1). The broad variations in composition of the silicates also testifies to the absence of strong thermal metamorphism during the evolution of the clast.

A distinctive textural feature of the clast is the presence of three cavities up to 0.3 mm across.

Detailed characteristics of clast d3A are presented in [5], along with a discussion of the processes responsible for its genesis, and here we consider only features of this clast related to the presence of the cavities and deposits in them.

The shape of the cavities can be very roughly described as rectangular, with smoothed corners. The elongation of the cavities (the ratio of their lengths to widths) varies from 1.1 to 1.6. The cavities are spatially restricted to porous portions of the clast. The walls of the cavities consist of relatively large olivine crystals, which compose a narrow zone of very high porosity. One of the cavities is partly rimmed with a set of elongated olivine crystals (bars), whose shapes obviously replicate the shape of the cavity wall (Fig. 2). The walls of the cavities are lined with a thin (visible thickness no more than 25 μm) usually zonal film.

Two of the three cavities in this clast additionally contain very thin elongated crystals, which are perpendicular to the walls of the cavity (Fig. 3). These crystals are characterized by the stripy structure. The maximum lengths of the crystals is approximately 25 μm at a thickness of <4 μm. The crystals extending into the free space of the cavity are covered with shells, whose thickness are comparable to those of the crystals themselves. Some of the crystals are completely surrounded with the film that lines the walls of the cavities.

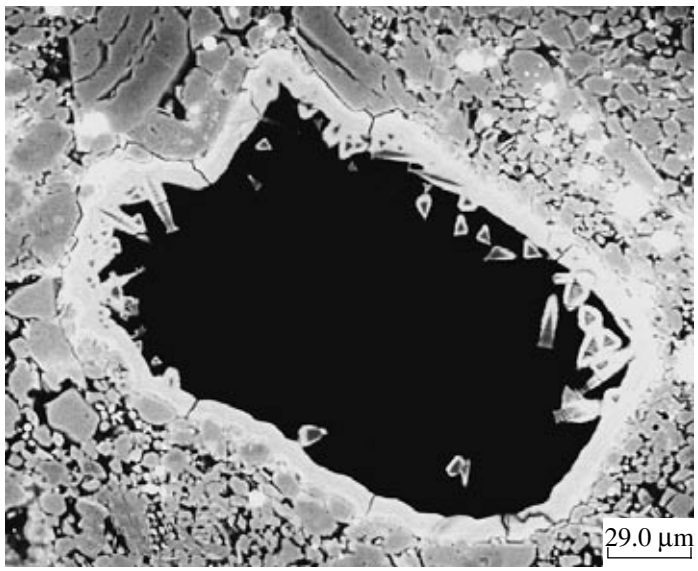

Fig. 2. Clast #d3A, cavity 1. The walls of the cavity consist of olivine crystals. The top of the image displays a stack of elongated olivine crystals. BSE image.

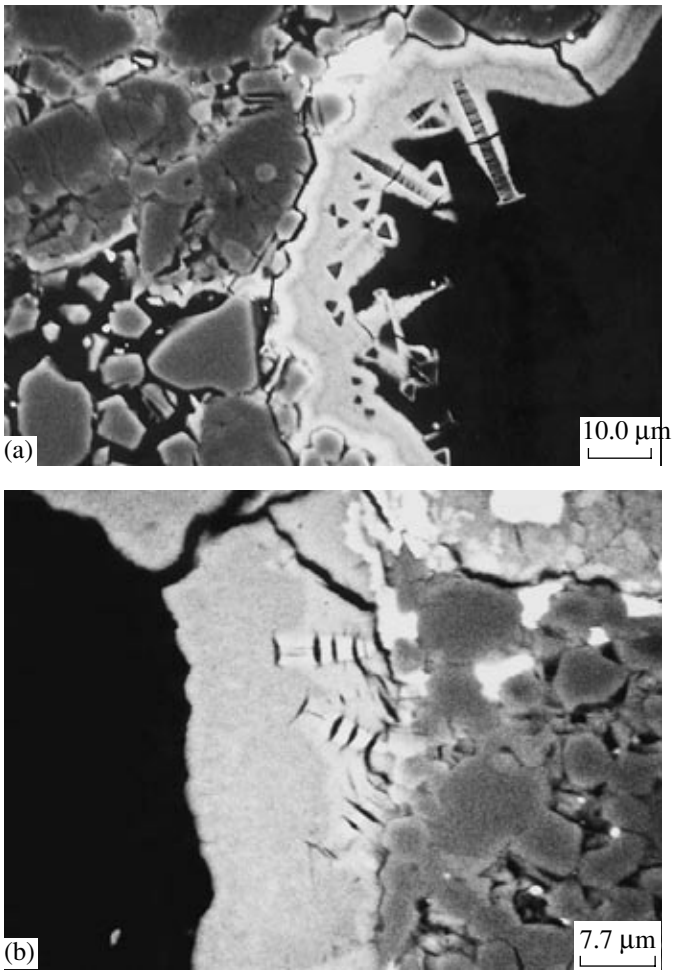

Fig. 3. Clast #d3A, blown-up images of cavities (a) 1 and (b) 2, showing the zonal structure of the coating on the walls of the cavities. Crystals in cavity 2 occur completely inside the coating. BSE images.

Table 2. Chemical composition (wt %) of objects in cavities of clast #3dA

No.	Object	SiO_2	TiO_2	Al_2O_3	Cr_2O_3	FeO	MnO	MgO	CaO	Na_2O	K_2O	S	P_2O_5	Total
1a	Coating of cavity 1*	30.7	0.29	12.0	0.15	30.0	0.36	9.61	0.09	0.15	0.27	0.53	0.13	84.28
1b	Coating of cavity 1*	32.6	<0.03	11.9	0.04	21.8	0.56	20.1	0.06	0.24	0.12	<0.03	0.14	86.01
2a	Coating of cavity 2*	27.6	0.12	11.0	0.11	37.4	0.21	8.13	0.12	0.50	0.46	0.23	0.17	86.05
2b	Coating of cavity 2*	34.7	<0.03	5.10	<0.03	31.4	0.24	14.7	0.04	0.27	0.21	<0.03	<0.03	86.66
3	Coating on a crystal from cavity 1 (n = 2)	32.9	<0.03	10.3	<0.03	22.1	0.62	19.1	0.07	0.10	0.08	<0.03	0.14	85.41
4	Crystals, analysis1**	3.46	<0.03	25.7	<0.03	23.1	0.12	35.3	<0.03	0.15	<0.03	<0.03	<0.03	87.83
5	Crystals, analysis2**	4.09	<0.03	24.8	<0.03	24.1	0.11	35.8	<0.03	0.14	<0.03	<0.03	<0.03	89.04
6	Crystals, analysis1***	–	–	27.5	–	23.3	–	37.4	–	–	–	–	–	88.2
7	Crystals, analysis2***	–	–	26.8	–	24.5	–	38.3	–	–	–	–	–	89.6

Note: n is the number of analyses; all Fe is recalculated to FeO.

* Representative analyses of the film lining the cavities, analyses a and b are from the same analytical profile: analysis a is the closest to the wall of the cavity, and analysis b is the closest to the cavity.

** Analyses of individual crystals.

*** Same analyses after subtracting the admixture of the material of the crystal coating, the MnO and Na_2O concentrations were ignored.

The chemical composition of the thin coating that lines the cavities is characterized by persistently low analytical totals (85–90 wt %) and corresponds to magnesian serpentine (Table 2). The compositions of the coatings somewhat differ from cavity to cavity and even within a single cavity, but thereby display a pervasive tendency in their variations; the concentrations of SiO_2, MgO, and MnO increase away from the walls of the cavity, whereas the contents of TiO_2, Al_2O_3, Cr_2O_3, FeO, Na_2O, K_2O, and S simultaneously decrease.

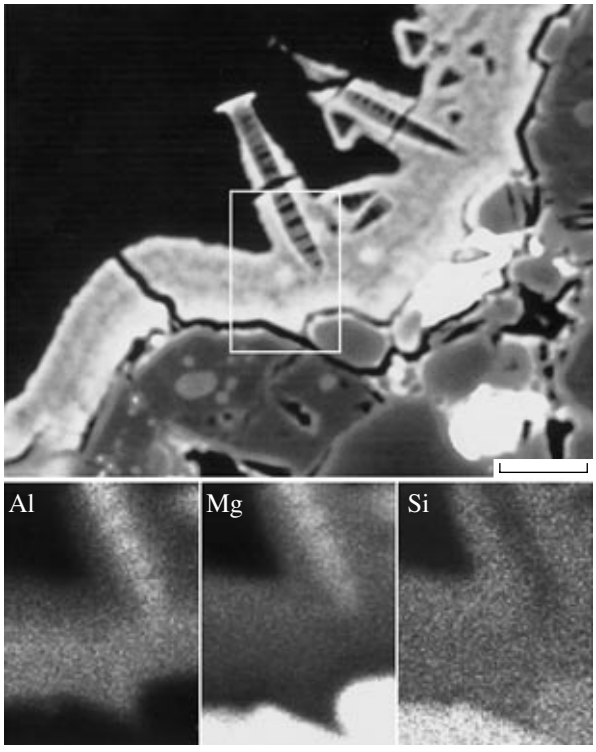

Fig. 4. BSE image of clast #d3A. The top image displays a large crystal in cavity 1. Scale bar is 10 μm long. The three bottom images show the area outlined in the top image; the images were taken in the k_α radiation of Al, Mg, and Si and demonstrate that the crystal is enriched in Al and Mg, and the coating Si.

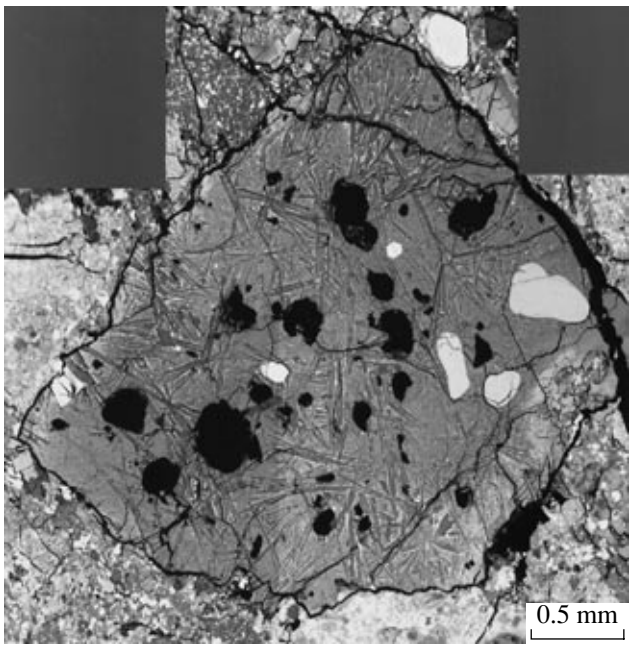

Fig. 5. Clast #d(3-5)D, thin section #d3. Black areas correspond to cavities, pale gray equant rounded grains are high-Ca pyroxenes, small white grains are apatite. The apatite grain at the top of the image has a subhedral hexagonal morphology with clear-cut angles and edges. BSE image.

We analyzed the largest crystal from cavity 1 and the coating around this crystal (Fig. 4). The microprobe analyses (Table 2) indicate that the analytical totals (of two analyses) for this crystal are persistently low, and its predominant components are Mg, Al, and Fe. The SiO_2 concentration is low and variable. Taking into consideration the very small sizes of this crystal, we are prone to believe that the presence of SiO_2 in the analyses was caused by the involvement of the neighboring shell in the analyses. Table 2 also presents the composition of the crystal from which the composition of the shell was subtracted, with the contribution of the latter to the analyses of the mineral estimated at 10–12% on the basis of the SiO_2 contents. The composition of the crystal calculated in this manner is stoichiometric and can be approximated by the formula $Mg_{11}Fe_4Al_6O_{24} \cdot nH_2O$. The composition of the shell covering the crystals is practically identical to the composition of the coating lining of the cavities (Table 2).

The cavities have sizes that are greater than the sizes of neighboring crystals and relatively "geometric" shapes. Obviously, these cavities could not be formed during the agglomeration of the clast. At the same time, the characteristics of the cavities led us to suggest that they developed in places occupied with some crystals previously, but these precursor crystals were lost during the subsequent evolution of the clast.

As was mentioned above, the aqueous alterations, which were related mostly to some process in the parent body, are typical of several fragments of the Kaidun meteorite. The results of this process can also be observed in the clast, for example, in the form of grains of a composition analogous to those of the alteration products of nickel-iron. Conceivably, the aqueous alterations were also responsible for the origin of the coating that lines the walls of the cavities. It is reasonable to suggest that the action of aqueous fluids also caused the dissolution of the precursor crystals and the origin of the cavities themselves. The spatial restriction of the cavities to the porous parts of the clast suggests that this porosity was also genetically related to the processes of aqueous alterations.

The very thin crystals in the cavities are in physical contact with the walls of the cavity. This suggests that the crystals started to grow before the origin of the coating that now covers the walls of the cavities. At the same time, the crystals are covered by shells, whose composition is close to that of the coating lining the cavity, but which are notably thinner than that. Obviously, the development rate of the coating was higher than the growth rate of the crystals, and this eventually resulted in the blocking of the growing crystals from the solution and the termination of the growth of these crystals. The zonal structure of the film lining the cavities is most probably explained by variations in the composition of the aqueous solution with time.

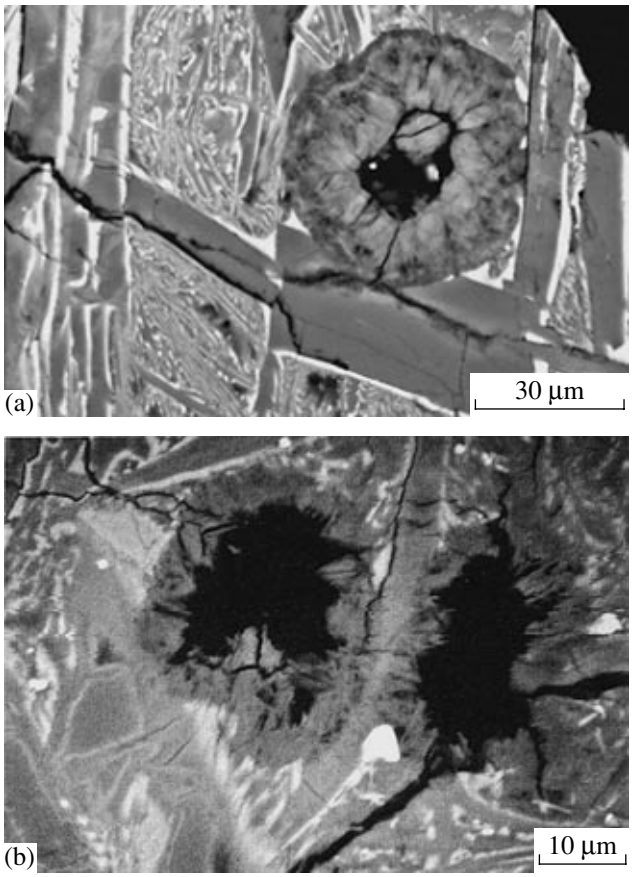

Fig. 6. Clast #d(3-5)D, cavities with (a) colloform (thin section #d4) and (b) crystalline (thin section #d3) coatings. BSE image.

CLAST #d(3-5)D

Clast #d(3-5)D is present in three polished thin sections (#d3, #d4, and #d5), which were obtained by subsequent cutting of the fragment of the Kaidun meteorite. The texture of the clast, its mineral composition, and the compositions of minerals are practically identical in all of the three thin sections. The texture of the clast is generally determined by laths of acid plagioclase submerged in a fine-grained groundmass of complex composition, which grades into vitreous material in the margins of the clast (Fig. 5). The clast contains single large crystals of apatite and pyroxenes. Opaque phases were not found.

Large pyroxene grains in this clast are of high- and low-Ca varieties, the apatite is Cl-apatite, the matrix plagioclase is sodic ($Ab_{76.7}An_{21.8}Or_{1.5}$ on average) and is rich in foreign components (TiO_2, FeO, MgO, and P_2O_5). The chemical composition of the main minerals of clast #d(3-5)D is presented in Table 3. Chemically, this clast as a whole is comparable with the terrestrial intermediate rocks of the subalkaline series, the family of trachyandesite.

The texture of the groundmass of clast #d(3-5)D of the Kaidun meteorite is fine-grained to vitreous, with

Table 3. Chemical composition (wt %, averages and ranges) of minerals in clast #d(3-5)D

Component	SiO_2	TiO_2	Al_2O_3	Cr_2O_3	FeO	MnO	MgO	CaO
Large grains								
Augite	52.2	0.28	0.89	0.92	12.8	0.51	14.6	17.1
$n = 35$	51.7–53.1	0.20–0.39	0.78–1.01	0.80–1.01	12.4–13.4	0.41–0.59	14.0–14.9	16.6–17.9
Pigeonite	51.8	0.62	0.42	0.20	26.0	0.61	16.1	4.69
$n = 5$	51.5–52.2	0.60–0.64	0.36–0.48	0.18–0.23	25.8–26.2	0.56–0.67	15.5–16.8	4.58–4.75
Apatite*	0.42	–	–	–	0.86	0.13	0.38	53.0
$n = 12$	0.35–0.51				0.76–0.93	0.08–0.18	0.30–0.44	51.6–53.9
Matrix minerals								
Plagioclase	62.6	0.08	23.1	<0.03	0.65	<0.03–0.05	0.34	4.86
$n = 19$	60.1–64.3	0.03–0.17	21.4–25.9		0.31–1.01		0.09–0.81	3.14–6.75
Pyroxene	48.0	1.67	2.69	0.24	23.2	0.91	10.4	10.0
$n = 6$	46.9–49.0	1.13–2.20	1.45–4.14	0.12–0.40	19.8–27.6	0.67–1.35	8.5–12.8	8.5–11.5
Anorthoclase**	66.5	–	20.1	–	0.99	–	1.23	1.71
Matrix***	58.1	0.53	16.9	0.06	6.89	0.19	2.89	4.55
$n = 136$	57.7–60.9	0.21–0.75	14.7–21.2	0.03–0.24	3.00–8.77	0.09–0.32	0.98–7.86	3.22–6.22

Component	Na_2O	K_2O	P_2O_5	Total	En or Ab	Wo or An	Fs or Or
Large grains							
Augite	0.42	<0.03	–	99.72	42.4	35.8	21.8
$n = 35$	0.35–0.58				41.4–43.2	35.1–37.1	21.1–22.7
Pigeonite	0.20	<0.03	–	100.64	46.8	9.8	43.4
$n = 5$	0.16–0.25				45.7–47.7	9.7–10.0	42.6–44.4
Apatite*	0.74	–	41.3	101.88*	–	–	–
$n = 12$	0.62–0.89		40.9–41.7				
Matrix minerals							
Plagioclase	8.52	0.22	0.12	100.49	74.5	24.2	1.3
$n = 19$	6.70–9.44	0.10–0.41	0.04–0.27		64.6–82.1	16.0–34.5	0.62–2.5
Pyroxene	0.91	0.07	1.32	99.41	33.3	23.2	43.5
$n = 6$	0.66–1.31	0.03–0.11	0.44–2.64		27.9–40.6	19.7–26.7	36.3–53.4
Anorthoclase**	8.53	1.88	–	100.94	79.6	8.8	11.6
Matrix***	7.41	0.49	0.92	98.93	–	–	–
$n = 136$	5.88–8.29	0.22–1.41	0.22–1.61				

Note: n is the number of analyses; all Fe is recalculated to FeO.
* Apatite additionally contains 3.10 wt % F and 1.95 wt % Cl.
**Representative analysis.
***Analysis by a microprobe beam defocused to 50×50 μm.

skeleton and sheath crystals of plagioclase and definitely suggests that the clast was produced during the rapid cooling of the melt. It was demonstrated in [6] that the cooling melt was in contact with the carbonaceous matrix. There are good reasons to believe that the clast was produced during a high-velocity impact event, with intense melting of the projectile material. However, the smoothed and rounded outlines of most of the large mineral grains in this clast are at variance with their origin during the crystallization of this melt and suggest the opposite process of the resorption of crystals in melt. Evidently, large mineral grains in this clast should be regarded as residues of a partly melted precursor fragment.

Clast #d(3-5)D is characterized by the presence of numerous cavities, whose walls are sometimes lined with a thin coating.

Clast #d(3-5)D itself and the processes responsible for its origin are described in much detail in [6], so here we consider only the features of this clast related to the occurrence of the cavities and deposits in them.

Table 4. Chemical composition (wt %, averages and ranges) of coatings in the cavities of clast #d(3-5)D

Coating no.	SiO_2	Al_2O_3	FeO	MnO	MgO	CaO
Colloform coating 1,	41.9	6.78	15.1	0.24	22.7	0.18
$n = 4$	39.9–43.3	6.51–7.09	14.6–15.8	0.22–0.26	22.2–23.2	0.16–0.19
Colloform coating 2,	42.5	12.0	8.80	0.50	25.8	0.16
$n = 5$	41.1–43.5	11.6–12.4	7.96–9.40	0.40–0.59	25.4–26.8	0.12–0.21
Crystalline coating 1*	6.05	19.1	23.2	0.16	25.0	0.06
Crystalline coating 2*	8.93	19.5	21.4	0.17	29.5	0.04
Crystalline coating 3*	8.71	22.4	22.6	0.20	28.8	0.08
Crystalline coating 1**	–	29.2	35.2	0.18	35.4	–
Crystalline coating 2**	–	28.7	31.0	0.16	40.1	–
Crystalline coating 3**	–	30.0	32.0	0.20	37.8	–

Coating no.	Na_2O	K_2O	S	P_2O_5	Total
Colloform coating 1,	0.59	0.21	0.13	<0.03	87.83
$n = 4$	0.50–0.71	0.20–0.22	0.11–0.13		
Colloform coating 2,	0.38	0.31	0.07	<0.03	90.52
$n = 5$	0.33–0.45	0.28–0.36	0.05–0.11		
Crystalline coating 1*	0.05	<0.03	0.09	0.04	73.75
Crystalline coating 2*	0.07	<0.03	0.17	0.05	79.83
Crystalline coating 3*	0.05	<0.03	0.15	0.10	83.09
Crystalline coating 1**	–	–	–	–	100
Crystalline coating 2**	–	–	–	–	100
Crystalline coating 3**	–	–	–	–	100

Note: n is the number of analyses; all Fe is recalculated to FeO. The TiO_2 and Cr_2O_3 concentrations are lower than 0.03 wt %.

* Microprobe analyses.

** Same analyses after subtracting the composition of the material of the colloform coating and renormalizing to 100%.

The sizes of the cavities in this clast range from a few tenths of a micrometer to ~0.5 mm. Large cavities usually have complicated ungeomeric morphologies. In places, plagioclase laths are truncated or cut across by such cavities. We found no systematic pattern in the arrangement of the cavities. Small cavities, less than ~100 μm across, are mostly (but not exclusively) restricted to finer crystalline portions of the groundmass. Small cavities are often rounded or elongated and spindle-shaped, and their walls are often lined by thin coatings.

The thickness of these coatings usually does not exceed 10 μm at a maximum of 18 μm (the latter can also be caused by the obliqueness of the cross section, which does not coincide with the diametral plane). The coatings can have textures of two types (Fig. 6): they can consist of aggregates of thin acicular crystals or be colloform. Thin crystalline coatings are restricted mostly to the marginal parts of the clast and were detected mostly in clast #d3D. Both types of the coatings can quite commonly occur in the same cavity, with the colloform coating overlying the crystalline one. The boundaries between the coatings are uneven and diffuse.

The coatings of the colloform type, which line the walls of small cavities, commonly have low analytical totals (85–92%) and consist of phyllosilicates of the chlorite–serpentine series (Table 4). The composition of these coatings notably varies from cavity to cavity, but remains relatively constant within a single cavity. Compositional zoning was not identified in any of them.

Fine-crystalline coatings are characterized (according to the data of three analyses) by high concentrations of MgO, FeO, and Al_2O_3 at quite low contents of SiO_2 and the near absence of almost all other analyzed components and low analytical totals (Table 4, Fig. 7). The latter fact is likely explained by the presence of water, which is confirmed by the instability of the material under an electron beam. At the same time, we also cannot rule out the influence of the defects of the analyzed surface. The low thickness of the thin-crystalline coatings, the occurrence of the overlying colloform coating, and the character of their boundary led us to explain the presence of SiO_2 by the involvement of the colloform material in the analyses. We subtracted the composition of the colloform coating from that of the fine-crystalline coating. The compositions thus calculated are in

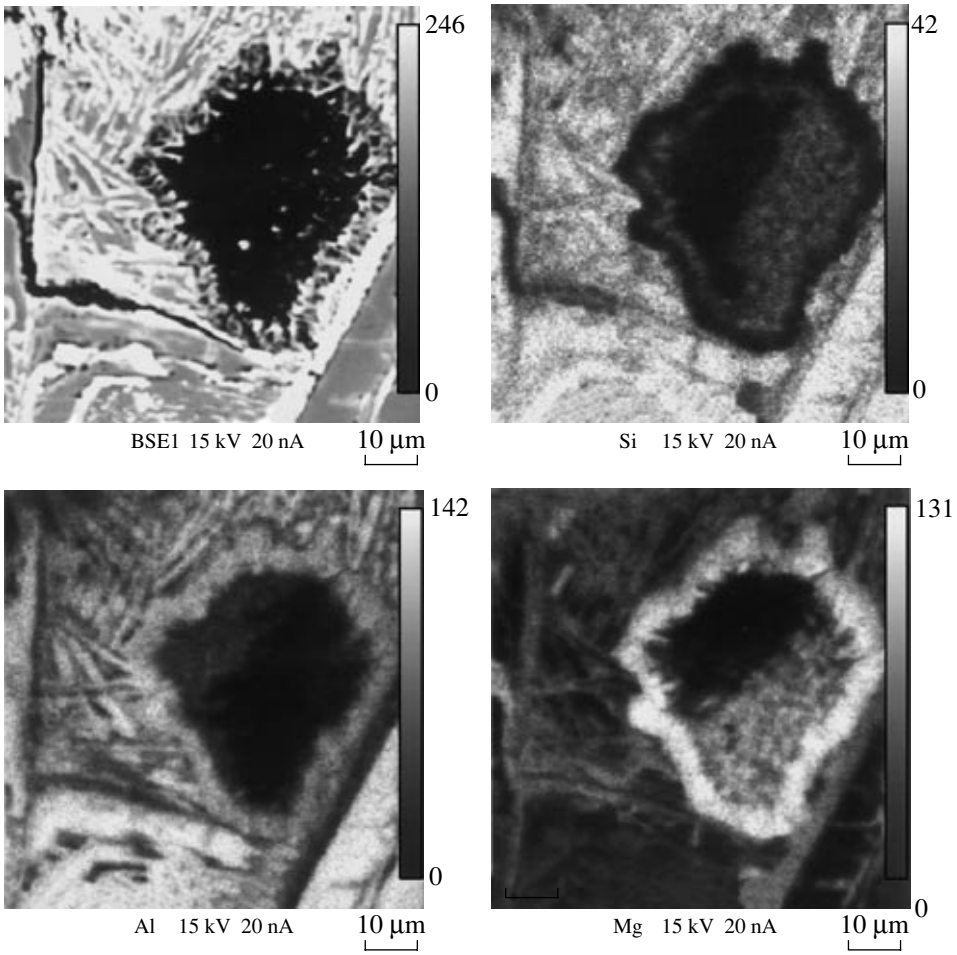

Fig. 7. Clast #d(3-5)D, a BSE image of a cavity with a crystalline coating and images of the same cavity in the k_α radiation of Al, Mg, and Si. The crystalline coating is enriched in Al and Mg but contains no Si, which is present only of the surface of crystals as a component of the colloform coating. Scale bar is 10 μm.

good agreement with the formula $(Mg,Fe,Mn)_5Al_2O_8 \cdot nH_2O$.

The coatings of both types contain minor amounts of sulfur, which was not detected in any other constituents of clast #d(3-5)D.

The origin of the cavities in this clast was likely related to the occurrence of a fluid phase that took place during cooling, simultaneously with the crystallization of the melt. This follows from the aforementioned breakup of the plagioclase laths by cavities, including those with coating on the walls.

The occurrence of a fluid phase can in principle be caused by contamination with water and other volatiles from the carbonaceous matrix of the meteorite. However, the melting and crystallization of the clast undoubtedly took place on or near the surface of the parent body, and it is hard to expect in this situation that any notable amounts of water and other volatiles could diffuse from the matrix of the meteorite into the melt that rapidly cooled under a very low pressure (space vacuum). The virtual absence of sulfur in the matrix of the clast and its very low iron concentration (both of these components are typical of the carbonaceous matrix of the meteorite) testifies that the contamination of the melt with the carbonaceous matrix material would be insignificant.

It is reasonable to believe that the presence of cavities in this clast was caused by the high contents of volatiles in the primary material of the clast.

The coatings on the walls of cavities in clast #d(3-5)D obviously originated during the latest stage of clast formation. The crystalline shells were formed before the colloform coatings, as follows from the aforementioned relative position of these shells on the walls of the cavities.

CONCLUSIONS

The crystalline coatings in the cavities of clast #d(3-5)D have the composition $(Mg,Fe,Mn)_5Al_2O_8 \cdot nH_2O$, which is closely similar (if not completely identical) to the composition of thin elongated individual crystals in

the cavities of clast #d3A ($Mg_{11}Fe_4Al_6O_{24} \cdot nH_2O$). The composition of the crystals from #d(3-5)D is presented in a more general form. The crystals of both of the clasts evidently crystallized from fluids of identical or closely similar composition and most probably of the same genesis.

The differences between the morphologies of this phase in clasts #d3A and #d(3-5)D (elongated individual crystals in the former and finely crystalline aggregates in the latter) were most probably caused by differences in the crystallization conditions. For example, the origin of numerous small crystals usually suggests a high temperature and concentration of the mineral-forming fluid, and, conversely, single large crystals grow from relatively cold and/or more diluted solutions.

The mineral in question in the partly remelted clast #d(3-5)D crystallized from a fluid, which was, perhaps, produced during the cooling of the melt that formed the clast itself. Clast #d3A has a chondritic texture and does not exhibits traces of noticeable thermal metamorphism. The phase grew in this clast from a fluid produced in clast #d(3-5)D, but at a lower temperature and/or concentration of the fluid.

The compositions of the phases (oxides and phyllosilicates) in the cavities led us to make some suggestions concerning the character of the mineral-forming fluid. The crystallization temperature of the mineral assemblages of carbonaceous chondrites (which are dominated by phyllosilicates) under the effect of aqueous solutions is estimated at 50–150°C [7]. The major components of the oxide phase is Mg and Al, and this seems to testify to an alkaline composition of the mineral-forming solution with a pH 8–10. Indeed, Mg is mobile in aqueous solutions at a pH not higher than 10.5, whereas amphoteric Al becomes mobile at a pH higher than 8 [8]. These estimates of pH are pertinent for room temperature, and analogous values at higher temperatures should be different.

The compositions of the phyllosilicates phases in the cavities of both of the clasts differ. These phases in the cavities of partly remelted clast #d(3-5)D, where the fluid was produced, are notably richer in SiO_2, MgO, CaO, Na_2O, and Cr_2O_3, but poorer in FeO than the phyllosilicates in the colloform coatings of clast #d3A (Tables 4 and 2, respectively). These compositional differences should also be explained by the changes in the characteristics of the mineral-forming fluid during its filtration.

A mineral phase of the composition $(Mg,Fe,Mn)_5Al_2O_8 \cdot nH_2O$ has never been found in nature before, a fact highlighting the unusual composition of the mineral-forming fluid. As was demonstrated above, the genesis of this fluid was related to partly remelted clast #d(3-5)D. The nature of this clast is really unusual: there are good reasons to believe that this clast is of Martian provenance [9].

ACKNOWLEDGMENTS

The authors thank M.A. Nazarov for useful discussion concerning several issues considered in this publication.

REFERENCES

1. A. V. Ivanov, N. N. Kononkova, and E. V. Guseva, "Hydrothermal Alterations of Schreibersite and Native Iron in the Meteorite Kaidun III (EH5)," Geokhimiya, No. 8, 1085–1093 (1992) [Geochem. Int. **30** (3), 11–19 (1993)].
2. A. V. Ivanov, G. Kurat, L. F. Migdisova, *et al.*, "The Kaidun Meteorite: Pre- and Postaccretionary Aqueous Alterations of Metal in an Enstatite Chondrite Fragment," Geokhimiya, No. 2, 131–136 (1998) [Geochem. Int. **36** (2), 101–106 (1998)].
3. A. V. Ivanov, M. E. Zolensky, F. Brandstaetter, *et al.*, "A Phyllosilicate–Sulfide Vein in Kaidun," Meteoritics **29**, 477 (1994).
4. M. K. Weisberg, M. Prinz, M. E. Zolensky, and A. V. Ivanov, "Carbonates in the Kaidun Meteorite," Meteoritics **29**, 549–550 (1994).
5. A. V. Ivanov, M. E. Zolensky, and S. V. Yang, "The Kaidun Meteorite: Evidence for Aqueous Alteration and Precipitation," Meteorit. Planet. Sci. **35** (Suppl.), A82 (2000).
6. A. V. Ivanov, N. N. Kononkova, S. V. Yang, and M. E. Zolensky, "The Kaidun Meteorite: Clasts of Alkaline-rich Fractionated Materials," Meteorit. Planet. Sci. **38**, 725–737 (2003).
7. M. E. Zolensky, W. L. Dourcier, and J. L. Gooding, "Aqueous Alteration on the Hydrous Asteroids: Results of EQ3/6 Computer Simulations," Icarus **78**, 411–425 (1989).
8. V. V. Shcherbina, *Principles of Geochemistry* (Nedra, Moscow, 1972) [in Russian].
9. A. V. Ivanov, "Is the Kaidun Meteorite a Sample from Phobos?," Astron. Vestn. **38** (2), 113–125 (2004) [Sol. Sys. Res., **38** (2), 97–107 (2004)].